

Article

# Synthesis, Antimicrobial Study, and Molecular Docking Simulation of 3,4-Dimethoxy- $\beta$ -Nitrostyrene Derivatives as Candidate PTP1B Inhibitor

Salman Alfarisi<sup>1</sup>, Mardi Santoso<sup>2</sup>, Alfinda Novi Kristanti<sup>1</sup>, Imam Siswanto<sup>1</sup>  
and Ni Nyoman Tri Puspaningsih<sup>1,3,\*</sup> 

<sup>1</sup> Department of Chemistry, Faculty of Science and Technology, Universitas Airlangga, Kampus C-UNAIR, Mulyorejo, Surabaya 60115, Indonesia; salman.alfarisi-2017@fst.unair.ac.id (S.A.); alfinda-n-k@fst.unair.ac.id (A.N.K.); imamsiswanto@fst.unair.ac.id (I.S.)

<sup>2</sup> Department of Chemistry, Faculty of Science and Data Analytics, Institut Teknologi Sepuluh Nopember, Kampus ITS, Sukolilo, Surabaya 60111, Indonesia; tsv09@chem.its.ac.id

<sup>3</sup> Proteomic laboratory, Research Center for Bio-Molecule Engineering, Universitas Airlangga, Kampus C-UNAIR, Mulyorejo, Surabaya 60115, Indonesia

\* Correspondence: ni-nyoman-t-p@fst.unair.ac.id; Tel.: +62-0811-345-2009

Received: 19 July 2020; Accepted: 3 September 2020; Published: 7 September 2020



**Abstract:** A derivative series of 3,4-dimethoxy- $\beta$ -nitrostyrene was synthesized through nitroaldol reaction, including a new compound of 3,4-ethylenedioxy- $\beta$ -bromo- $\beta$ -nitrostyrene. The antimicrobial activity effect of 3,4-alkyloxy modification of  $\beta$ -nitrostyrene was investigated. A molecular docking study was also performed to obtain information about their interactions with protein tyrosine phosphatase 1B (PTP1B). The active residues of cysteine-215 and arginine-221 of PTP1B play a key role in signaling pathways that regulate various microorganism cell functions. It also acts as a negative regulator in signaling pathways of insulin that are involved in type 2 diabetes and other metabolic diseases. These derivatives exhibited potential antifungal activity. The studied compounds were also had potential as fragments to be PTP1B inhibitors by interacting with serine-216 and arginine-221 residues, according to their molecular docking. 3,4-Ethylenedioxy- $\beta$ -methyl- $\beta$ -nitrostyrene was the most successful potential candidate as a PTP1B inhibitor. However, further research is needed to investigate their potential for medicinal use.

**Keywords:** 3,4-dimethoxy- $\beta$ -nitrostyrene derivatives; antimicrobial agent; PTP1B; molecular docking

## 1. Introduction

The frequency of invasive, systemic fungal infections has increased dramatically, with worsening disease severity and higher incidence rates worldwide. Unfortunately, few antifungal drugs that are currently available for the treatment of systemic mycoses are ideal in terms of antifungal spectrum, efficacy, and safety. Many classes of drug structures are currently used to fight fungal infections, such as azoles, polyenes, pyrimidine analogs, and echinocandins (Figure 1). The increase in incidences of fungal infections has been accompanied by an increase in antifungal drug resistance. This is exacerbated by the fact that a new generation of antifungals is lagging behind the rate at which fungal infections develop [1,2]. This encourages the widening of the hunt for the development of new antifungal agents from several derivative compounds. One of which is the possibility of developing drugs from  $\beta$ -nitrostyrene derivatives.

Compounds containing a  $\beta$ -nitrostyrene fragment have been described as having bioactivity [3]. Several  $\beta$ -nitrostyrene compounds have recently been examined as anticancer candidates. The identified pharmacophore is the nitroethenyl side chain of the aromatic ring. Research on the antifungal and

antibacterial activities of this frame of structures during the most recent decade is rather rare, even though studies in this field have been conducted since the 1940s. In many cases, the  $\beta$ -nitrostyrene structures were known to be more active against Gram-positive bacteria than other types of bacteria [3].

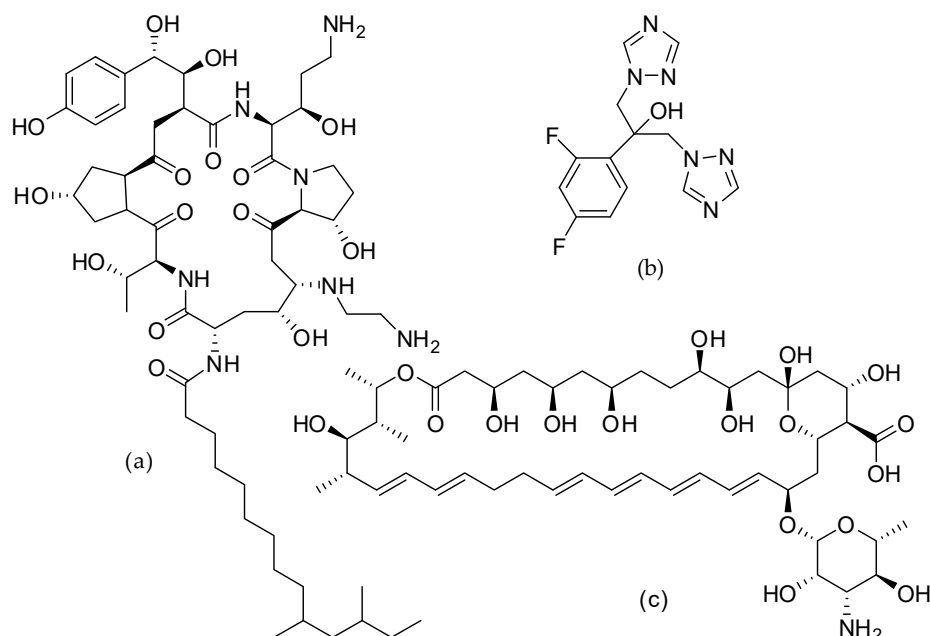


**Figure 1.** Representative antifungal drugs from several classes. (a) Caspofungin; (b) Fluconazole; (c) Nystatin.

Park and Pei argued that  $\beta$ -nitrostyrene is a reversible tyrosine phosphatase inhibitor, inhibiting and interfering with protein tyrosine phosphatases (PTPs) to restrain cell signaling in microorganisms. Eukaryotic tyrosine phosphorylation controls normal cellular growth, cell-to-cell communication, cell differentiation, cell migration, and gene transcription. Bacterial protein tyrosine phosphatases have structural and sequential similarities to their eukaryotic counterparts but are not as specialized as the protein tyrosine phosphatases of eukaryotes. The nitrovinyl chain of  $\beta$ -nitrostyrene acts as a phosphotyrosine mimetic to inhibit protein tyrosine phosphatase 1B (PTP1B) through binding interaction with Cys215 at the active site of the protein [4–6].

PTP1B, a member of the PTP family, is a major negative regulator of the signaling pathways they are involved in [7]. PTP1B consists of 435 amino acids and is located at the endoplasmic reticulum, with a molecular weight of 50 kDa and a PTP family-owned conservative sequence. The phosphatase catalytic site of PTP1B is localized along the sequence of residues from histidine 214 to arginine 221 in the p fold, in which the critical residues of its active sites are Cys215 and Arg221 [8].

Based on the diversity of PTP1B inhibitory mechanisms, several classes of synthetic compounds and natural products have been characterized for development as therapeutic agents [9]. Even so, inventing selective PTP1B inhibitors that possess good pharmacological aspects is difficult, which is why there are no PTP1B-qualified inhibitors yet to be found in clinical trials. The basic challenge to finding a new inhibitor structure for PTP1B involves its acting as a phosphotyrosine mimetic with adequate selectivity, very low toxicity and high bioavailability [10]. Fragment-based drug design is a new approach to determining the initial chemical starting point for drug discovery projects. The small fragments make the optimization that follows, to create a molecule by exploring the chemical cavity in the binding pocket, relatively easier [11]. For this reason, small molecules of PTP1B inhibitors could be promising candidate drugs in the design of new therapeutic agents against bacterial or fungal infections. Clearly,  $\beta$ -nitrostyrene derivatives can be considered as fragments for the design of drugs.

Computer-aided docking is a significant tool for understanding binding interactions between a ligand and its protein target. It is a sophisticated method for drug design, and small molecules docking to the known protein structures has become an integral part of the drug discovery process [12]. In the last few years, various virtual screening approaches have been developed to predict the inhibitor activity of PTP1B. Moreover, studies of molecular docking to representative inhibitors have been conducted to investigate the binding pose of inhibitors at the active sites of PTP1B. The results of docking studies indicate that the studied compounds form hydrogen bonds with residues such as Arg24, Tyr46, Asp48, Asp181, Ser216, Gly220, Arg221, Arg254, and Gln262 [13,14]. To date, studies on the molecular docking of  $\beta$ -nitrostyrene derivatives against PTP1B have not been carried out.

PTP1B also plays a key role as a negative regulator in the insulin-signaling pathways involved in type 2 diabetes. The enzyme interacts with insulin receptors as well as substrate-1 of insulin receptors, thereby dephosphorylating phosphotyrosine residues and effecting down-regulation of insulin action. Type 2 drives the global pandemic, with an ever-increasing numbers of patients, accounting for 90% of all diabetes cases [9,15]. In addition, PTP1B overexpression has been implicated in the signaling of cancer, tumor and in inflammation processes [16–18]. Therefore, PTP1B is also an attractive drug candidate for the therapy of type 2 diabetes and other metabolic diseases.

Several studies have reported that  $\beta$ -nitrostyrene derivatives were successfully prepared for biological purposes. However, only a few studies were related to the bioactivity effect of side chain conformation of the aromatic ring of  $\beta$ -nitrostyrene compounds, and a study of alkyloxy chains has not yet been conducted. In the present work, several 3,4-dimethoxy- $\beta$ -nitrostyrene derivatives were synthesized as antimicrobial agents that correlate with inhibition of PTP1B (Figure 2). In this series, the alkyloxy chain at position 3,4 of  $\beta$ -nitrostyrene was modified. Modifications of substituent at  $\beta$ -carbon of  $\beta$ -nitrostyrene were also made to investigate the effect of structural changes on their activity. The antimicrobial activity of the derivatives was assessed and docking simulations of them into the catalytic site of PTP1B were also performed to compare the results.

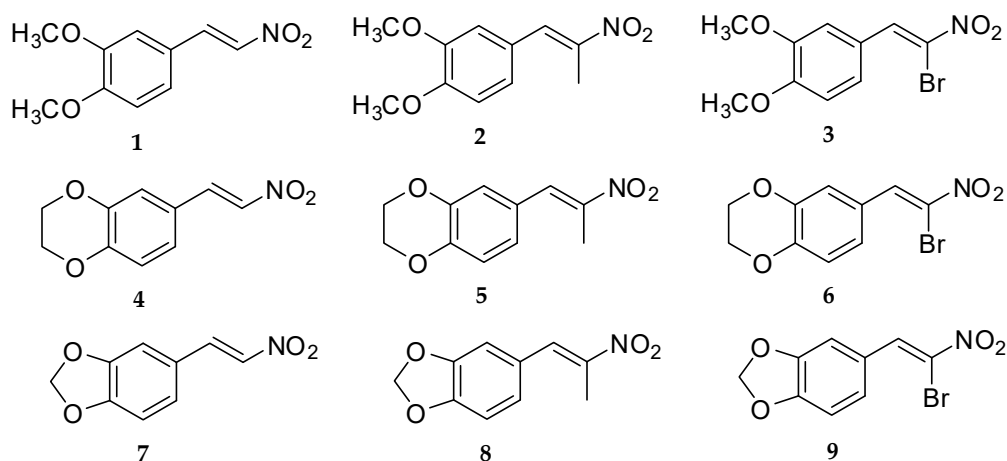


**Figure 2.** 3,4-Dimethoxy- $\beta$ -nitrostyrene derivatives synthesized in the study. The number (1–9) was used to represent the name of the compounds.

## 2. Materials and Methods

The major chemicals were obtained from Sigma-Aldrich (St. Louis, MO, USA). Thin layer chromatography and column chromatography were performed using Merck 60 F<sub>254</sub> silica gel and 60 (70–230 mesh) silica gel, respectively (Darmstadt, Germany). FT-IR spectroscopy was conducted using a Bruker ALPHA spectrometer with Ge-ATR (Billerica, MA, USA). <sup>1</sup>H- and <sup>13</sup>C-NMR analysis was carried out using a JEOL JNM ECS-400 spectrometer (Tokyo, Japan) in deuterated chloroform at 400 MHz. Mass spectroscopy was performed on an Agilent 5977B MSD-7890 GC System (Santa Clara, CA, USA). High Resolution Mass Spectrometry (HRMS) was carried out using Waters Xevo

QToF MS (Milford, MA, USA). Melting points were measured using a Fisher-Johns apparatus and are uncorrected. All commercial reagents and solvents used were of analytical grade.

## 2.1. Synthesis of 3,4-Dimethoxy- $\beta$ -Nitrostyrene Derivatives

### 2.1.1. Synthesis of $\beta$ -Nitrostyrene Series

The methods of Mee et al. [19], were slightly modified and adapted for the synthesis of the compounds. The corresponding aldehyde was dissolved in stirred glacial acetic acid. Ammonium acetate and nitromethane ( $\rho = 1.14 \text{ g/cm}^3$ ) were added, then the mixture was refluxed while stirring for 2 h at 50 °C (reaction progress monitored by TLC). The dark orange mixture was cooled to room temperature, and distilled water was added. The crude orange product was filtered off, washed with water, then extracted with dichloromethane. The phase of organic extract was dried over  $\text{MgSO}_4$ , filtered, and evaporated under a vacuum. The yellow solid was recrystallized twice from ethanol to yield the product, with the melting point being determined and identified through spectrometric analysis.

**Compound 1:** A mixture of 3,4-dimethoxybenzaldehyde (2.29 g, 14 mmol) and nitromethane (15.96 g, 256 mmol) with ammonium acetate (3.70 g, 48 mmol) in glacial acetic acid (5 mL) was reacted, and light yellow crystals were obtained, 1.48 g, 50.5% yield, mp 139 °–141 °C. FT-IR (ATR;  $\nu$ ,  $\text{cm}^{-1}$ ): 1491 (asymmetric  $\text{NO}_2$ ), 1358 (symmetric  $\text{NO}_2$ );  $^1\text{H}$  NMR (400 MHz,  $\text{CDCl}_3$ ):  $\delta_{\text{H}}$  (ppm): 7.94 (1H, d,  $J = 13.6 \text{ Hz}$ , H- $\beta$ ), 7.52 (1H, d,  $J = 13.6 \text{ Hz}$ , H- $\alpha$ ), 7.16 (1H, dd,  $J = 2.0, 8.0 \text{ Hz}$ , H-6), 6.99 (1H, d,  $J = 2.0 \text{ Hz}$ , H-2), 6.89 (1H, d,  $J = 8.8 \text{ Hz}$ , H-5), 3.92 (3H, s, C3-OCH<sub>3</sub>), 3.91 (3H, s, C4-OCH<sub>3</sub>);  $^{13}\text{C}$  NMR (400 MHz,  $\text{CDCl}_3$ )  $\delta_{\text{C}}$  (ppm): 152.9 (C-3), 149.6 (C-4), 139.4 (C- $\alpha$ ), 135.2 (C- $\beta$ ), 124.7 (C-1), 122.9 (C-6), 111.4 (C-5), 110.3 (C-2), 56.2 (C3-OCH<sub>3</sub>), 56.1 (C4-OCH<sub>3</sub>); GC/MS  $m/z$  (%): 209 (M, 100), 162 (51), 119 (14), 91 (16). HRMS:  $\text{C}_{10}\text{H}_{11}\text{NO}_4\text{Na}$  [ $\text{M}+\text{Na}$ ] $^+$ ; calculated: 232.0586, found: 232.0604.

**Compound 4:** A mixture of 3,4-ethylenedioxybenzaldehyde (1.29 g, 8 mmol) and nitromethane (9.12 g, 146 mmol) with ammonium acetate (2.11 g, 27.4 mmol) in glacial acetic acid (3 mL) was reacted, and light yellow crystals were obtained, 1.20 g, 72.5% yield, mp 147 °–149 °C. FT-IR (ATR;  $\nu$ ,  $\text{cm}^{-1}$ ): 1509 (asymmetric  $\text{NO}_2$ ), 1338 (symmetric  $\text{NO}_2$ );  $^1\text{H}$  NMR (400 MHz,  $\text{CDCl}_3$ ):  $\delta_{\text{H}}$  (ppm): 7.89 (1H, d,  $J = 13.2 \text{ Hz}$ , H- $\beta$ ), 7.46 (1H, d,  $J = 13.6 \text{ Hz}$ , H- $\alpha$ ), 7.06 (1H, d,  $J = 2.4 \text{ Hz}$ , H-2), 7.05 (1H, d,  $J = 6.8 \text{ Hz}$ , H-5), 6.90 (1H, dd,  $J = 2.4, 6.4 \text{ Hz}$ , H-6), 4.33–4.27 (2H, m, C3-OCH<sub>2</sub>), 4.33–4.27 (2H, m, C4-OCH<sub>2</sub>);  $^{13}\text{C}$  NMR (400 MHz,  $\text{CDCl}_3$ )  $\delta_{\text{C}}$  (ppm): 147.5 (C-4), 144.1 (C-3), 139.1 (C- $\alpha$ ), 135.6 (C- $\beta$ ), 123.6 (C-1), 123.5 (C-6), 118.4 (C-5), 117.9 (C-2), 64.8 (C3-OCH<sub>2</sub>), 64.2 (C4-OCH<sub>2</sub>); GC/MS  $m/z$  (%): 207 (M, 100), 160 (66), 89 (26), 77 (19). HRMS:  $\text{C}_{10}\text{H}_9\text{NO}_4\text{Na}$  [ $\text{M}+\text{Na}$ ] $^+$ ; calculated: 230.0429, found: 230.0439.

**Compound 7:** A mixture of 3,4-methylenedioxybenzaldehyde (1.18 g, 8 mmol) and nitromethane (9.12 g, 146 mmol) with ammonium acetate (2.11 g, 27.4 mmol) in glacial acetic acid (4 mL) was reacted, and brownish yellow crystals were obtained, 0.80 g, 52% yield, mp 158 °–160 °C. FT-IR (ATR;  $\nu$ ,  $\text{cm}^{-1}$ ): 1492 (asymmetric  $\text{NO}_2$ ), 1332 (symmetric  $\text{NO}_2$ );  $^1\text{H}$  NMR (400 MHz,  $\text{CDCl}_3$ ):  $\delta_{\text{H}}$  (ppm): 7.91 (1H, d,  $J = 13.6 \text{ Hz}$ , H- $\beta$ ), 7.46 (1H, d,  $J = 13.6 \text{ Hz}$ , H- $\alpha$ ), 7.07 (1H, dd,  $J = 1.6, 7.6 \text{ Hz}$ , H-6), 6.99 (1H, d,  $J = 1.6 \text{ Hz}$ , H-2), 6.86 (1H, d,  $J = 8.0 \text{ Hz}$ , H-5), 6.05 (2H, s, C3-OCH<sub>2</sub>O-C4);  $^{13}\text{C}$  NMR (400 MHz,  $\text{CDCl}_3$ )  $\delta_{\text{C}}$  (ppm): 151.5 (C-3), 148.8 (C-4), 139.2 (C- $\alpha$ ), 135.5 (C- $\beta$ ), 126.8 (C-1), 124.2 (C-6), 109.2 (C-2), 107.1 (C-5), 102.2 (C3-OCH<sub>2</sub>O-C4); GC/MS  $m/z$  (%): 193 (M, 92), 146 (100), 89 (61), 63 (31). HRMS:  $\text{C}_9\text{H}_7\text{NO}_4\text{Na}$  [ $\text{M}+\text{Na}$ ] $^+$ ; calculated: 216.0273, found: 216.0269.

### 2.1.2. Synthesis of $\beta$ -Methyl- $\beta$ -Nitrostyrene Series

The corresponding aldehyde was dissolved in stirred glacial acetic acid. Ammonium acetate and nitroethane ( $\rho = 1.045 \text{ g/cm}^3$ ) were added, then the mixture was refluxed while stirring for 2 h at 50 °C (reaction progress monitored by TLC). The dark orange mixture was then cooled to room temperature, extracted with dichloromethane, and washed with distilled water. The layer of organic extract was dried over  $\text{MgSO}_4$  then filtered and concentrated under a vacuum. The crude orange solid was recrystallized twice from ethanol to yield the product, with the melting point determined and identified using spectrometric analysis.

**Compound 2:** A mixture of 3,4-dimethoxybenzaldehyde (1.66 g, 10 mmol) and nitroethane (14.63 g, 200 mmol) with ammonium acetate (2.71 g, 35 mmol) in glacial acetic acid (5 mL) was reacted, and light yellow crystals were obtained, 1.26 g, 56.5% yield, mp 66 °–68 °C. FT-IR (ATR;  $\nu$ ,  $\text{cm}^{-1}$ ): 1511 (asymmetric  $\text{NO}_2$ ), 1313 (symmetric  $\text{NO}_2$ );  $^1\text{H}$  NMR (400 MHz,  $\text{CDCl}_3$ ):  $\delta_{\text{H}}$  (ppm): 8.06 (1H, s, H- $\alpha$ ), 7.08 (1H, dd,  $J = 2.0, 8.8$  Hz, H-6), 6.94 (1H, d,  $J = 2.4$  Hz, H-2), 6.93 (1H, d,  $J = 8.4$  Hz, H-5), 3.93 (3H, s, C3-OCH<sub>3</sub>), 3.91 (3H, s, C4-OCH<sub>3</sub>), 2.48 (3H, s, H- $\gamma$ );  $^{13}\text{C}$  NMR (400 MHz,  $\text{CDCl}_3$ )  $\delta_{\text{C}}$  (ppm): 150.8 (C-3), 149.1 (C-4), 133.9 (C- $\alpha$ ), 145.9 (C- $\beta$ ), 125.1 (C-1), 124.1 (C-6), 113.1 (C-5), 111.3 (C-2), 56.1 (C3-OCH<sub>3</sub>), 56.1 (C4-OCH<sub>3</sub>), 14.3 (C- $\gamma$ ); GC/MS  $m/z$  (%): 223 (M, 100), 176 (51), 131 (25), 91 (16). HRMS:  $\text{C}_{11}\text{H}_{13}\text{NO}_4\text{Na}$   $[\text{M}+\text{Na}]^+$ ; calculated: 246.0742, found: 246.0735.

**Compound 5:** A mixture of 3,4-ethylenedioxybenzaldehyde (0.70 g, 4.3 mmol) and nitroethane (8.36 g, 100 mmol) with ammonium acetate (2.00 g, 26 mmol) in glacial acetic acid (5 mL) was reacted, and light yellow crystals were obtained, 0.28 g, 30.3% yield, mp 73 °–75 °C. FT-IR (ATR;  $\nu$ ,  $\text{cm}^{-1}$ ): 1503 (asymmetric  $\text{NO}_2$ ), 1284 (symmetric  $\text{NO}_2$ );  $^1\text{H}$  NMR (400 MHz,  $\text{CDCl}_3$ ):  $\delta_{\text{H}}$  (ppm): 7.98 (1H, s, H- $\alpha$ ), 6.98 (1H, d,  $J = 2.0$  Hz, H-2), 6.96 (1H, dd,  $J = 2.0, 8.4$  Hz, H-6), 6.91 (1H, d,  $J = 8.4$  Hz, H-5), 4.32–4.27 (2H, m, C3-OCH<sub>2</sub>), 4.32–4.27 (2H, m, C4-OCH<sub>2</sub>), 2.44 (3H, s, H- $\gamma$ );  $^{13}\text{C}$  NMR (400 MHz,  $\text{CDCl}_3$ )  $\delta_{\text{C}}$  (ppm): 146.2 (C-4), 145.5 (C-3), 133.6 (C- $\alpha$ ), 143.7 (C- $\beta$ ), 125.7 (C-1), 124.4 (C-6), 119.2 (C-5), 117.9 (C-2), 64.7 (C3-OCH<sub>2</sub>), 64.3 (C4-OCH<sub>2</sub>), 14.2 (C- $\gamma$ ); GC/MS  $m/z$  (%): 221 (M, 100), 174 (78), 103 (38), 91 (29). HRMS:  $\text{C}_{11}\text{H}_{11}\text{NO}_4\text{Na}$   $[\text{M}+\text{Na}]^+$ ; calculated: 244.0586, found: 244.0575.

**Compound 8:** A mixture of 3,4-methylenedioxybenzaldehyde (1.50 g, 10 mmol) and nitroethane (14.63 g, 200 mmol) with ammonium acetate (2.71 g, 35 mmol) in glacial acetic acid (5 mL) was reacted and light yellow crystals were obtained, 0.99 g, 47.6% yield, mp 88 °–90 °C. FT-IR (ATR;  $\nu$ ,  $\text{cm}^{-1}$ ): 1508 (asymmetric  $\text{NO}_2$ ), 1319 (symmetric  $\text{NO}_2$ );  $^1\text{H}$  NMR (400 MHz,  $\text{CDCl}_3$ ):  $\delta_{\text{H}}$  (ppm): 8.01 (1H, s, H- $\alpha$ ), 6.97 (1H, dd,  $J = 2.0, 8.0$  Hz, H-6), 6.93 (1H, d,  $J = 1.2$  Hz, H-2), 6.88 (1H, d,  $J = 8.0$  Hz, H-5), 6.04 (2H, s, C3-OCH<sub>2</sub>O-C4), 2.45 (3H, s, H- $\gamma$ );  $^{13}\text{C}$  NMR (400 MHz,  $\text{CDCl}_3$ )  $\delta_{\text{C}}$  (ppm): 149.4 (C-3), 148.3 (C-4), 133.8 (C- $\alpha$ ), 146.2 (C- $\beta$ ), 126.3 (C-1), 126.1 (C-6), 109.6 (C-2), 108.9 (C-5), 101.9 (C3-OCH<sub>2</sub>O-C4), 14.3 (C- $\gamma$ ); GC/MS  $m/z$  (%): 207 (M, 83), 160 (87), 103 (100), 77 (43). HRMS:  $\text{C}_{10}\text{H}_9\text{NO}_4\text{Na}$   $[\text{M}+\text{Na}]^+$ ; calculated: 230.0429, found: 230.0431.

### 2.1.3. Synthesis of $\beta$ -Bromo- $\beta$ -Nitrostyrene Series

The corresponding aldehyde was dissolved in stirred glacial acetic acid. Ammonium acetate and bromo-nitromethane ( $\rho = 2.007 \text{ g/cm}^3$ ) were added, then the mixture was refluxed while stirring for 2 h at 50 °C (reaction progress monitored by TLC). The dark orange mixture was cooled to room temperature then extracted with dichloromethane and washed with distilled water. The organic extracts were dried over  $\text{MgSO}_4$ , filtered, and concentrated under a vacuum. The crude residue was purified using column chromatography over silica gel with eluent of n-hexane-chloroform (1:4) to yield the product with the melting point determined and identified through spectrometric analysis.

**Compound 3:** A mixture of 3,4-dimethoxybenzaldehyde (0.92 g, 5.5 mmol) and bromo-nitromethane (2.01 g, 12.9 mmol) with ammonium acetate (0.70 g, 9 mmol) in glacial acetic acid (1.5 mL) was reacted, and orange crystals were obtained, 0.31 g, 19.6% yield, mp 110 °–112 °C. FT-IR (ATR;  $\nu$ ,  $\text{cm}^{-1}$ ): 1517 (asymmetric  $\text{NO}_2$ ), 1307 (symmetric  $\text{NO}_2$ );  $^1\text{H}$  NMR (400 MHz,  $\text{CDCl}_3$ ):  $\delta_{\text{H}}$  (ppm): 8.63 (1H, s, H- $\alpha$ ), 7.59 (1H, d,  $J = 2.4$  Hz, H-2), 7.51 (1H, dd,  $J = 2.0, 8.8$  Hz, H-6), 6.96 (1H, d,  $J = 8.8$  Hz, H-5), 3.95 (3H, s, C3-OCH<sub>3</sub>), 3.93 (3H, s, C4-OCH<sub>3</sub>);  $^{13}\text{C}$  NMR (400 MHz,  $\text{CDCl}_3$ )  $\delta_{\text{C}}$  (ppm): 152.7 (C-3), 149.0 (C-4), 136.7 (C- $\alpha$ ), 127.0 (C-1), 125.5 (C-6), 122.7 (C- $\beta$ ), 112.8 (C-5), 111.1 (C-2), 56.2 (C3-OCH<sub>3</sub>), 56.1 (C4-OCH<sub>3</sub>); GC/MS  $m/z$  (%): 289 (M,  $^{81}\text{Br}$ , 55), 287 (M,  $^{79}\text{Br}$ , 56), 162 (100), 147 (45), 91 (29). HRMS:  $\text{C}_{10}\text{H}_{10}\text{NO}_4\text{NaBr}$   $[\text{M}+\text{Na}]^+$ ; calculated: 309.9691, found: 309.9687.

**Compound 6:** A mixture of 3,4-ethylenedioxybenzaldehyde (0.90 g, 5.5 mmol) and bromo-nitromethane (2.61 g, 17 mmol) with ammonium acetate (0.70 g, 9 mmol) in glacial acetic acid (2 mL) was reacted, and light yellow crystals were obtained, 0.90 g, 57.3% yield, mp 129 °–131 °C. FT-IR (ATR;  $\nu$ ,  $\text{cm}^{-1}$ ): 1509 (asymmetric  $\text{NO}_2$ ), 1277 (symmetric  $\text{NO}_2$ );  $^1\text{H}$  NMR (400 MHz,  $\text{CDCl}_3$ ):  $\delta_{\text{H}}$  (ppm): 8.55 (1H, s, H- $\alpha$ ), 7.59 (1H, d,  $J = 1.6$  Hz, H-2), 7.39 (1H, dd,  $J = 2.4, 8.8$  Hz, H-6), 6.95 (1H, d,  $J = 8.8$  Hz,

H-5), 4.34–4.28 (2H, m, C3-OCH<sub>2</sub>), 4.34–4.28 (2H, m, C4-OCH<sub>2</sub>); <sup>13</sup>C NMR (400 MHz, CDCl<sub>3</sub>) δ<sub>C</sub> (ppm): 147.4 (C-4), 143.7 (C-3), 136.3 (C-α), 126.3 (C-1), 125.9 (C-β), 123.3 (C-6), 119.8 (C-5), 117.9 (C-2), 64.8 (C3-OCH<sub>2</sub>), 64.2 (C4-OCH<sub>2</sub>); GC/MS *m/z* (%): 287 (M, <sup>81</sup>Br, 51), 285 (M, <sup>79</sup>Br, 53), 160 (100), 104 (45), 76 (35). HRMS: C<sub>10</sub>H<sub>8</sub>NO<sub>4</sub>NaBr [M+Na]<sup>+</sup>; calculated: 307.9534, found: 307.9537.

Compound **9**: A mixture of 3,4-methylenedioxybenzaldehyde (1.66 g, 11 mmol) and bromonitromethane (4.82 g, 30 mmol) with ammonium acetate (1.4 g, 18 mmol) in glacial acetic acid (4 mL) was reacted, and brown crystals were obtained, 0.61 g, 20.3% yield, mp 93 °–95 °C. FT-IR (ATR; ν, cm<sup>-1</sup>): 1495 (asymmetric NO<sub>2</sub>), 1295 (symmetric NO<sub>2</sub>); <sup>1</sup>H NMR (400 MHz, CDCl<sub>3</sub>) δ<sub>H</sub> (ppm): 8.58 (1H, s, H-α), 7.62 (1H, d, *J* = 1.6 Hz, H-2), 7.34 (1H, dd, *J* = 1.2, 8.0 Hz, H-6), 6.91 (1H, d, *J* = 8.0 Hz, H-5), 6.08 (2H, s, C3-OCH<sub>2</sub>O-C4); <sup>13</sup>C NMR (400 MHz, CDCl<sub>3</sub>) δ<sub>C</sub> (ppm): 151.2 (C-3), 148.3 (C-4), 136.5 (C-α), 129.1 (C-1), 125.8 (C-6), 124.1 (C-β), 109.4 (C-2), 108.9 (C-5), 102.2 (C3-OCH<sub>2</sub>O-C4); GC/MS *m/z* (%): 273 (M, <sup>81</sup>Br, 32), 271 (M, <sup>79</sup>Br, 32), 226 (<sup>81</sup>Br, 30), 224 (<sup>79</sup>Br, 30), 146 (100). HRMS: C<sub>9</sub>H<sub>6</sub>NO<sub>4</sub>NaBr [M+Na]<sup>+</sup>; calculated: 293.9378, found: 293.9382.

## 2.2. Antimicrobial Assay

The minimum inhibitory concentration (MIC) for bacteria, yeast, and mold was set in Mueller–Hinton Broth at 18 h, 24 h, and 5 d, respectively. The strains used for biological tests were: *Staphylococcus aureus*, *Pseudomonas aeruginosa*, *Candida albicans*, and *Aspergillus niger*. The inoculum was prepared by fitting a suspension to match 0.2 optical density (OD) at 600 nm. Broth microdilution testing was adapting to National Committee for Clinical Laboratory Standards guidelines. The test compounds were prepared in DMSO 2% at various concentrations. Microplate assays for bacterial and yeast were performed in clear using 96-well plates. The test compounds were applied to the plates, each containing 100 μL media, with a total volume of 200 μL per well. The microplates were incubated 24 h at 30 °C aerobically before the wells were read visually for turbidity. Disk diffusion assay for a mold was performed. A swab dipped into the standardized inoculums was scratched evenly on plates containing Mueller–Hinton (MH) agar. Suspension disks containing 20 uL of test compounds were added to the surfaces of the inoculated plates. The plates were then incubated at 30 °C for 5 days to allow for fungal growth. The zone diameter of inhibition was measured in millimeters. The positive controls used in this assay were ciprofloxacin for bacteria, nystatin for yeast and griseofulvin for mold. All assays were at least twice replicated. MIC results were reported as MIC (μg/mL) for standards. The compounds were evaluated for activity. Statistical analyses were performed using MS Excel 2007.

## 2.3. Molecular Docking

Molecular docking was conducted using Autodock 4.2 which is supported by Autodock Tools 1.5.6 and MGL tools. The crystal structure of PTP1B (PDB ID 1XBO) was extracted from the PDB server (<http://www.rcsb.org/pdb>). The receptor native–ligand complex was pre-processed using UCSF Chimera 1.14. Accelrys Discovery Studio 2.1 and Chem3D Ultra 10.0 were used for ligand preparation and supported protein optimization. Determination of the residues in the active site was used to analyze the dimensions of the grid box. Docking validation was undertaken by analyzing the root-mean-square deviation (RMSD) between the native ligand structure and the residues in the active site of the protein structure. 3,4-Dimethoxy-β-nitrostyrene derivatives were docked using Autodock 4.2 in a flexible manner. Visualization of bonding interactions was generated using UCSF Chimera 1.14 and PyMol 2.0 [12,20].

## 2.4. Molecular Dynamic Simulation

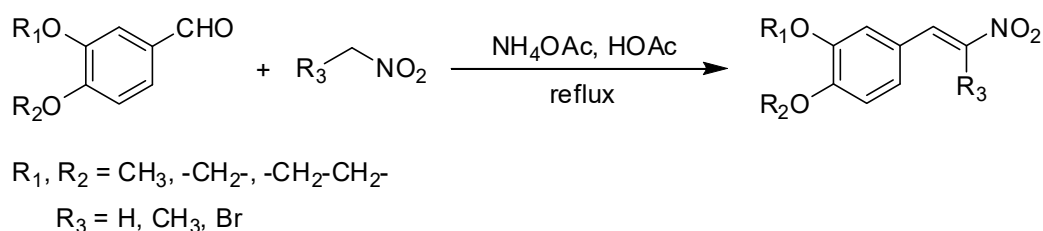
Molecular dynamic simulation was performed using Amber Molecular Dynamic package program for 100 ns simulation. A post-processing procedure was applied to calculate binding free energy between receptor and each ligand calculation was carried out. Binding energy calculation was carried out using MMPBSA.py module which is included in Amber Molecular Dynamic Package Program [21,22]. Atomic partial charge was added to each atom of the receptor using molecular

mechanic (MM) methods with the AMBER ff14SB force field, while to each atom of the ligand using semiempirical methods AM1-BCC [23].

### 3. Results and Discussion

#### 3.1. Spectroscopic Analysis

3,4-Dimethoxy- $\beta$ -nitrostyrene derivatives were synthesized through nitroaldol reaction (Scheme 1). Spectroscopy analysis indicated that the spectral data from nuclear magnetic resonance and mass spectrometry were compatible with the structures suggested. NMR and GCMS analysis of the 3,4-dimethoxy- $\beta$ -nitrostyrene derivatives suggested that the  $\beta$ -*E*-nitrostyrene conformation was predominant in most of the compounds synthesized. For example, for compound **2** the *E/Z* ratio is 45/2.



**Scheme 1.** General synthesis of 3,4-dimethoxy- $\beta$ -nitrostyrene derivatives.

#### 3.2. Antimicrobial Activity

Compound **2** was used for the preliminary assay to investigate the antimicrobial potency of the 3,4-dimethoxy- $\beta$ -nitrostyrene derivatives by their activity against strains of bacteria, yeast, and mold. The most inhibited strain was selected for the subsequent assay. The MIC result of compound **2** is displayed in Table 1. The second assay was used to evaluate the possible systemic anti-infective agents of the 3,4-dimethoxy- $\beta$ -nitrostyrene derivatives (as the MIC for each compound), and the results are displayed in the Table 2.

**Table 1.** Antimicrobial activity of compound **2** against several microbial strains.

Strain	Minimum Inhibitory Concentration ( $\mu\text{g/mL}$ )
<i>Staphylococcus aureus</i>	>128
<i>Pseudomonas aeruginosa</i>	>128
<i>Candida albicans</i>	128
<i>Aspergillus niger</i>	256
Ciprofloxacin (The positive control of <i>Staphylococcus aureus</i> )	>256
Ciprofloxacin (The positive control of <i>Pseudomonas aeruginosa</i> )	>256
Nystatin (The positive control of <i>Candida albicans</i> )	20
Griseofulvin (The positive control of <i>Aspergillus niger</i> )	>300

The antimicrobial assays (Table 1) indicated that compound **2** displayed potential broad activity. Among the microbial strains, its highest activity was against *Candida albicans* (MIC of 128  $\mu\text{g/mL}$ ). An analysis of the turbidity indicated that compound **2** was also more potent against *Staphylococcus aureus* (gram-positive bacteria) than *Pseudomonas aeruginosa* (gram-negative bacteria) (data not shown). The MIC results of antimicrobial activity against *Candida albicans* for the 3,4-dimethoxy- $\beta$ -nitrostyrene derivatives are displayed in Table 2, with MICs ranging from 32 to 128  $\mu\text{g/mL}$ . Compounds **4** and **7** were more active than compound **1**. Between compounds **3**, **6**, and **9**, 3,4-ethylenedioxy- $\beta$ -bromo- $\beta$ -nitrostyrene was the most active compound against *Candida albicans*. Among compounds **2**, **5**, and **8**, the 3,4-ethylenedioxy- $\beta$ -methyl- $\beta$ -nitrostyrene was clearly superior. Therefore, the ethylenedioxy group in position 3,4- of the benzene ring gave a stronger inhibitory effect than the methylenedioxy or dimethoxy groups. The 3,4-dimethoxy series were the weakest

agents, and they showed almost identical results in activity against *Candida albicans*. Among the 3,4-ethylenedioxy series, **4** and **5** were more effective, but there was little difference in their activity. Between compounds **7**, **8**, and **9**, 3,4-methylenedioxy- $\beta$ -nitrostyrene was the most active compound against *Candida albicans*. Thus, the  $\beta$ -methyl or  $\beta$ -bromine group at the nitrovinyl chain induce the decrease in the inhibitory effect. However, the fact that **5** was superior to **6** indicated that, in this case,  $\beta$ -methyl substitution leads to higher activity than  $\beta$ -bromo substitution. Indeed, in previous studies, several antimicrobial assays were carried out with compounds **1**, **2**, **7**, and **8** against several strains with varying MIC values [3–6].

**Table 2.** Antimicrobial activity of the 3,4-dimethoxy- $\beta$ -nitrostyrene derivatives against *Candida albicans*.

Compound	Minimum Inhibitory Concentration ( $\mu\text{g/mL}$ )
3,4-Dimethoxy- $\beta$ -nitrostyrene ( <b>1</b> )	128
3,4-Dimethoxy- $\beta$ -methyl- $\beta$ -nitrostyrene ( <b>2</b> )	128
3,4-Dimethoxy- $\beta$ -bromo- $\beta$ -nitrostyrene ( <b>3</b> )	128
3,4-Ethylenedioxy- $\beta$ -nitrostyrene ( <b>4</b> )	32
3,4-Ethylenedioxy- $\beta$ -methyl- $\beta$ -nitrostyrene ( <b>5</b> )	32
3,4-Ethylenedioxy- $\beta$ -bromo- $\beta$ -nitrostyrene ( <b>6</b> )	64
3,4-Methylenedioxy- $\beta$ -nitrostyrene ( <b>7</b> )	32
3,4-Methylenedioxy- $\beta$ -methyl- $\beta$ -nitrostyrene ( <b>8</b> )	128
3,4-Methylenedioxy- $\beta$ -bromo- $\beta$ -nitrostyrene ( <b>9</b> )	128
Nystatin as positive control	20

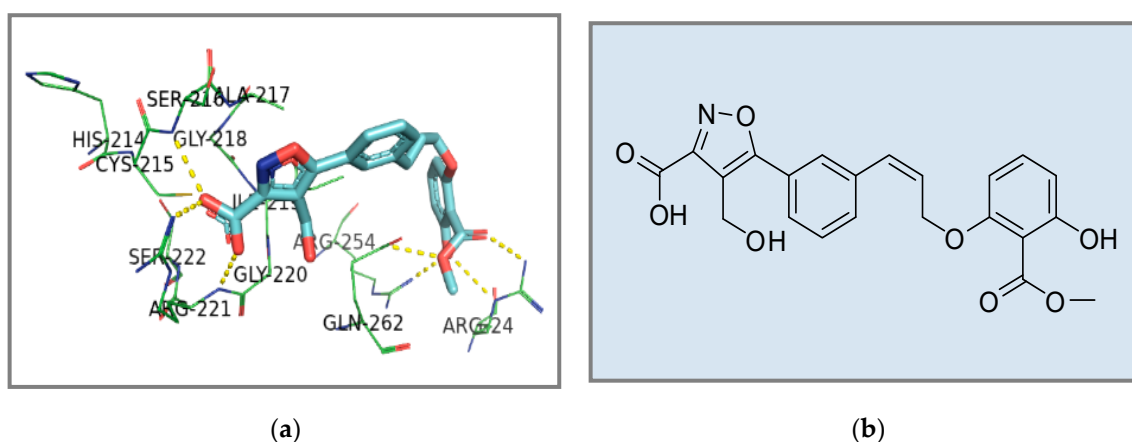
The higher activity of some 3,4-dimethoxy- $\beta$ -nitrostyrene derivatives might indicate that they acted as tyrosine mimetics, interacting with tyrosine phosphatase and interrupting cell signaling in the strains. Tyrosine phosphorylation in eukaryotes such as *Candida albicans* controls cell differentiation, cell migration, and gene transcription. These enzymes are also involved in other cellular processes, such as cell wall synthesis, the formation of hyphae, and maintenance of cellular integrity in stress situations. Tyrosine phosphorylation are also known to be involved in mitogen-activated protein kinase signaling cascades. The mitogen-activated protein kinase cascade in *Candida albicans* can trigger the transition of budding yeast to form more invasive filamentous yeast [4,24,25].

Park and Pei proposed that the tyrosine phosphatase was PTP1B. They also argued that  $\beta$ -nitrostyrene compounds inhibit PTP1B through their interaction and formation of a covalent complex with Cys215 residue at the active site [4]. In order to learn more about the interaction of 3,4-dimethoxy- $\beta$ -nitrostyrene derivatives on their binding pocket with PTP1B, molecular docking with conformational analysis was carried out.

### 3.3. Molecular Docking

Docking validation was performed to gain the best geometry of ligand–protein by re-docking the original ligand to the receptor. The best result in RMSD analysis between the native ligand structures and the residues of the receptor active site is 1.36 Å. The interaction between them is displayed in Figure 3.

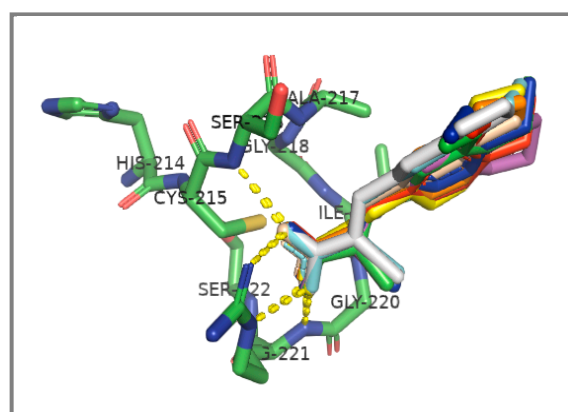
The results of docking analysis (Table 3) show that 3,4-dimethoxy- $\beta$ -nitrostyrene derivatives form H-bonds with the 1XBO amino acids Ser216 and Arg221 and that they were around the active site residues of 1XBO (Figure 4).



**Figure 3.** (a) protein tyrosine phosphatase 1B PTP1B (1XBO) amino acid residues around the original ligand; (b) the native ligand structure. The colors represent the element or atom (Red: Oxygen; Blue: Nitrogen; Yellow: Sulphur; Orange: Phosphor; Green: Carbon of the receptor residues; Cyan: Carbon of ligand; Dotted Yellow line: Interaction between the atoms).

**Table 3.** Binding energies calculated for the compounds by using Autodock 4.2.

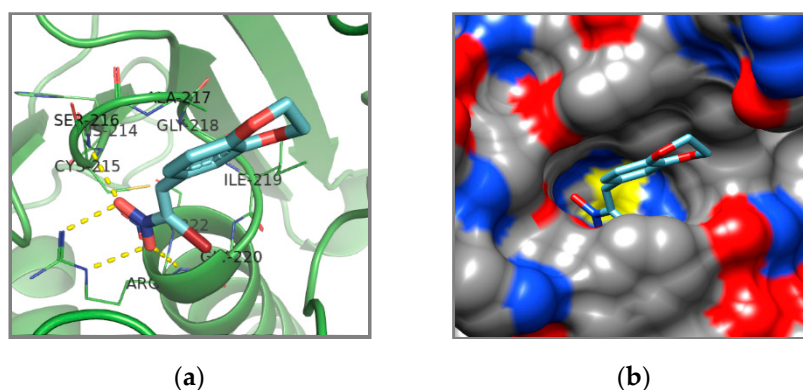
Compound	Binding Energy (kcal/mol)	Inhibition Constant	Hydrogen Binding Interacting Residues
Native ligand	−10.35	25.78 nM	Arg24, Ser216, Arg221, Arg254, Gly262
1	−7.36	4.04 μM	Ser216, Arg221
2	−8.13	1.09 μM	Ser216, Arg221
3	−8.47	615.90 nM	Ser216, Arg221
4	−7.77	2.03 μM	Ser216, Arg221
5	−8.42	672.70 nM	Ser216, Arg221
6	−8.81	348.98 nM	Ser216, Arg221
7	−7.41	3.71 μM	Ser216, Arg221
8	−8.02	1.33 μM	Ser216, Arg221
9	−8.45	643.05 nM	Ser216, Arg221



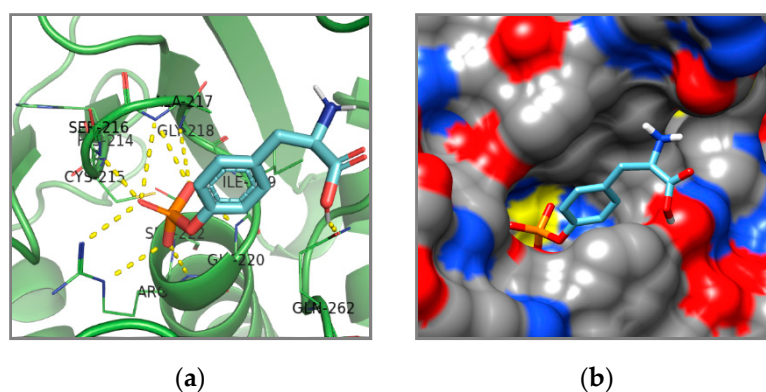
**Figure 4.** Molecular docking related PTP1B inhibition by 3,4-dimethoxy-β-nitrostyrene derivatives. Binding sites of compounds 1, 2, 3, 4, 5, 6, 7, 8, and 9 are represented by red, green, blue, yellow, magenta, cyan, orange, tint, and gray structures, respectively. The figure was generated using PyMol 2.0.

The results of the binding energy calculation from the docking analysis of the 3,4-dimethoxy-β-nitrostyrene derivative compounds on 1XBO showed that the new compound 6 was the best docking structure, with a binding energy of −8.81 kcal/mol. The detailed binding site of compound 6 is displayed in Figure 5. Four H-bonds were formed by compound 6 with Arg221, while only one H-bond was formed with Gly216. The nitro group of compound 6 binds to the Arg221 residue via hydrogen bonding interactions involving α-NH<sub>2</sub>, δ-NH, δ-NH, and ω-NH<sub>2</sub> with bond distances of 1.915, 2.384,

1.837 and 1.629 Å, respectively. It also forms an H-bond with Gly216 residue involving  $\alpha$ -NH<sub>2</sub> and a bond distance of 1.795 Å. To compare it with the inhibitory ability of compound **6**, phosphorylated tyrosine, which acts as substrate of PTP1B in the living system, was also docked. The result is displayed in Figure 6. The binding energy and inhibition constant of the substrate were  $-8.34$  kcal/mol and 772.7 nM, respectively. It forms H-bonds with the 1XBO amino acids Ser216, Ala217, Gly220, and Arg221.



**Figure 5.** Docking result of compound **6** in the PTP1B catalytic site. (a) Key residues surrounding **6**; (b) Binding pose of **6**. The colors represent the element or atom (Red: Oxygen; Blue: Nitrogen; Yellow: Sulphur; Orange: Phosphor; Green: Carbon of the receptor residues; Cyan: Carbon of ligand; Dotted Yellow line: Interaction between the atoms).

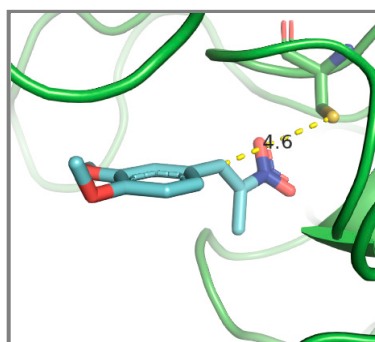


**Figure 6.** Docking result of phosphorylated tyrosine in the PTP1B catalytic site (a) Key residues; (b) Binding pose. The colors represent the element or atom (Red: Oxygen; Blue: Nitrogen; Yellow: Sulphur; White: Hydrogen; Orange: Phosphor; Green: Carbon of the receptor residues; Cyan: Carbon of ligand; Dotted Yellow line: Interaction between the atoms).

The docking results indicate that all the docked compounds are around the active site residues of 1XBO (214–221 residues), the critical acids of catalytic sites are Cys215 and Arg221 [5]. They showed interaction with Arg221 residue, whereas none was observed with Cys215 residue. An interaction between a molecule with a Cys215 residue can occur via Michael addition, in which sulfhydryl groups of cysteine act as attractive nucleophiles to the conjugated nitroalkene as acceptors [5]. This occurs if the distance between the sulfur of Cys215 and the  $\alpha$ -carbon of 3,4-dimethoxy- $\beta$ -nitrostyrene derivatives is suitable to making C-S bonds (i.e.,  $<1.82$  Å) [26,27]. The bond distances between them were determined using PyMol 2.0 (Table 4), the distances are relatively large. Therefore, the compounds may not be able to interact with Cys215. Even so, the  $\alpha$ -carbon of compounds **2** and **5** was closer to the sulfur of Cys215 than that of the others (Figure 7).

**Table 4.** Bond distance between  $\alpha$ -carbon of all compounds and the sulfur of Cys215, calculated using PyMol 2.0.

Compound	Bond Distance (Å)
1	4.9
2	4.6
3	4.7
4	4.9
5	4.6
6	4.9
7	4.8
8	4.7
9	4.9

**Figure 7.** Bond distance between  $\beta$ -carbon of compound 2 and thiol of Cys215, simulated using PyMol 2.0. The colors represent the element or atom (Red: Oxygen; Blue: Nitrogen; Yellow: Sulphur; Orange: Phosphor; Green: Carbon of the receptor residues; Cyan: Carbon of ligand; Dotted Yellow line: Interaction between the atoms).

### 3.4. Molecular Dynamic Simulation

In order to validate the calculation which resulted from previous molecular docking procedure, a molecular dynamic simulation was applied to all compound docked complexes to 100 ns. The results of calculation of binding energies are displayed in the Table 5.

**Table 5.** Binding energies calculated for the compounds after 100 ns molecular dynamic simulation.

Compound	Binding Energy (kcal/mol)
1	-11.69
2	-20.21
3	-15.13
4	-20.52
5	-16.79
6	-12.97
7	-10.61
8	-12.60
9	-10.21

Compound 4 exhibited the best docking structure, with binding energy of  $-20.52$  kcal/mol. However, compounds 2 and 5 were the promising most potential candidates for the PTP1B inhibitors according to the result of binding energies from the two methods of calculation. The hydrogen bonds of the two structures might stabilize the open shape of the enzyme and supply tighter binding to the PTP1B active site, so that inhibition of PTP1B becomes more effective.

### 3.5. Conformational Analysis

The conformational analysis showed that the side chain of the aromatic ring and substituent of the  $\beta$ -carbon of  $\beta$ -nitrostyrene chain affect the direction of the nitro group so that it is in the appropriate position to bind with hydrogen. The most stable geometries of molecular conformation before and after molecular docking, are displayed in Figure 8. The change in direction of the nitro group relative to the benzene was investigated by determining the dihedral angles between their planes, which are relatively greater based on the order of the substituent in  $\beta$ -carbon:  $H < CH_3 < Br$  (Table 6). Of course, this corresponds to binding energy. The magnitude of the angle was calculated from the dihedral angles of  $C_6-C_1-C_\alpha-C_\beta$  and  $C_\alpha-C_\beta-N-O$ .

**Table 6.** Dihedral angles of the nitro group relative to the benzene calculated using Chem3D Ultra 10.0.

Compound	Angle (°)
1	41
2	54
3	37
4	31
5	49
6	66
7	34
8	45
9	61

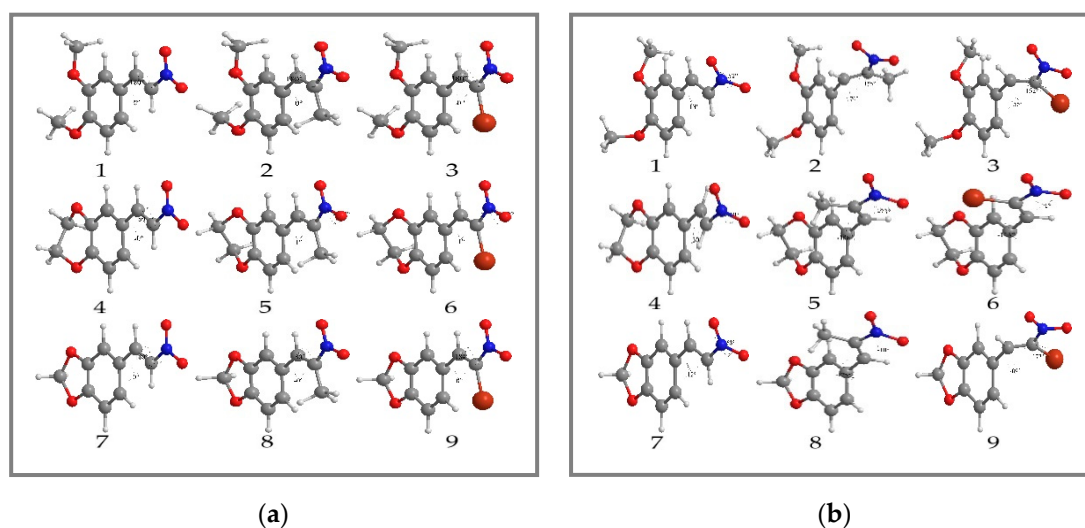


**Figure 8.** (a) Conformation for each compound in the most stable geometries before molecular docking; (b) After molecular docking. The colors represent the element or atom (Red: Oxygen; Blue: Nitrogen; White: Hydrogen; Gray: Carbon; Dark red: Bromine)

In general, the ethylenedioxy group in position 3,4 of benzene ring provided relatively more inhibitory effect than the methylenedioxy or methoxy groups. The results of this docking study support the results regarding antimicrobial activity against *Candida albicans*. It is also possible to propose that compound 5 is the best candidate PTP1B inhibitor as an antimicrobial agent among the studied compounds. The theoretical prediction of the toxicity of these derivatives supports the proposal that compound 5 is less toxic than the others. The predictions were processed using the pkCSM online tool available at <http://biosig.unimelb.edu.au/pkcsm/prediction> and the results are displayed in Table 7. However, further study is required to prove this argument.

**Table 7.** Toxicity data for 3,4-dimethoxy- $\beta$ -nitrostyrene derivatives (acquired using pkCSM online tool).

Compound	AMES Toxicity (Yes/No)	Max. Tolerated Dose (Human) (Log mg/kg/day)	hERG Inhibitor (Yes/No)	Oral Rat Acute Tox. (LD50) (mol/kg)	Hepato-Toxicity (Yes/No)	Skin Sensitization (Yes/No)
1	Yes	0.847	No	2.170	No	Yes
2	Yes	0.889	No	2.211	No	Yes
3	Yes	0.845	No	2.464	No	No
4	Yes	0.546	No	2.289	No	Yes
5	No	0.342	No	2.382	No	No
6	Yes	0.597	No	2.316	No	No
7	Yes	0.614	No	2.352	No	Yes
8	No	0.405	No	2.432	No	Yes
9	Yes	0.664	No	2.345	No	No

#### 4. Conclusions

The 3,4-dimethoxy- $\beta$ -nitrostyrene derivatives were suggested to have potential antifungal activity, especially against *Candida albicans*. The molecular docking study also suggested that 3,4-dimethoxy- $\beta$ -methyl- $\beta$ -nitrostyrene and 3,4-ethylenedioxy- $\beta$ -methyl- $\beta$ -nitrostyrene have activity as PTP1B inhibitors. Modification of the alkyloxy side chain at 3,4 position of the aromatic ring had significant influence on antifungal activity of  $\beta$ -nitrostyrenes. The most promising potential inhibitor was 3,4-ethylenedioxy- $\beta$ -methyl- $\beta$ -nitrostyrene.

**Author Contributions:** Conceptualization, S.A., N.N.T.P., M.S. and A.N.K.; methodology, M.S., N.N.T.P., I.S. and S.A.; investigation, S.A.; writing—original draft preparation, S.A.; validation, S.A., N.N.T.P., M.S., I.S. and A.N.K.; writing—review and editing, N.N.T.P.; supervision, N.N.T.P. All authors have read and agreed to the published version of the manuscript.

**Funding:** This study was funded by the Ministry of Religious Affairs (MORA), Indonesia.

**Acknowledgments:** Salman Alfarisi acknowledge to UNAIR Research University (Research Group Grant, Universitas Airlangga, Rector Decree 347/UN3.14/PT/2020) and MORA, Indonesia for the PhD scholarship program.

**Conflicts of Interest:** The authors declare no conflict of interest. The funders had no role in the design of the study; in the collection, analyses, or interpretation of data; in the writing of the manuscript, or in the decision to publish the results.

#### References

- Shapiro, R.S.; Robbins, N.; Cowen, L.E. Regulatory circuitry governing fungal development, drug resistance, and disease. *Microbiol. Mol. Biol. Rev.* **2011**, *75*, 213–267. [[CrossRef](#)] [[PubMed](#)]
- Khabnadideh, S.; Rezaei, Z.; Pakshir, K.; Zomorodian, K.; Ghafari, N. Synthesis and antifungal activity of benzimidazole, benzotriazole and aminothiazole derivatives. *Res. Pharm. Sci.* **2012**, *7*, 65–72.
- Milhazes, N.; Calheiros, R.; Marques, M.P.M.; Garrido, J.; Cordeiro, M.N.D.S.; Rodrigues, C.; Quinteira, S.; Novais, C.; Peixe, L.; Borges, F.  $\beta$ -Nitrostyrene derivatives as potential antibacterial agents: A structure-property-activity relationship study. *Bioorg. Med. Chem.* **2006**, *14*, 4078–4088. [[CrossRef](#)]
- Nicoletti, G.; Cornell, H.; Hügel, H.M.; White, K.S.; Nguyen, T.; Zalisniak, L.; Nugegoda, D. Synthesis and antimicrobial activity of nitroalkenylarenes. *Anti-Infect. Agents* **2013**, *11*, 179–191. [[CrossRef](#)]
- Cornell, H.; Nguyen, T.; Nicoletti, G.; Jackson, N.; Hügel, H.M. Comparison of halogenated  $\beta$ -nitrostyrene as antimicrobial agents. *Appl. Sci.* **2014**, *4*, 380–389. [[CrossRef](#)]
- Lo, K.; Cornell, H.; Nicoletti, G.; Jackson, N.; Hügel, H.M. A study of fluorinated  $\beta$ -nitrostyrene as antimicrobial agents. *Appl. Sci.* **2012**, *2*, 114–128. [[CrossRef](#)]
- Tonks, N.K. PTP1B: From the sidelines to the front lines! *FEBS Lett.* **2003**, *546*, 140–148. [[CrossRef](#)]
- Sun, J.; Qu, C.; Wang, Y.; Huang, H.; Zhang, M.; Li, H.; Zhang, Y.; Wang, Y.; Zou, W. PTP1B, a potential target of type 2 diabetes mellitus. *Mol. Biol.* **2016**, *5*, 174. [[CrossRef](#)]
- Tamrakar, A.K.; Maurya, C.K.; Rai, A.K. PTP1B inhibitor for type 2 diabetes treatment: A patent review (2011–2014). *Expert Opin. Ther. Patents* **2014**, *24*, 1–15. [[CrossRef](#)]
- Verma, M.; Gupta, S.J.; Chaudhary, A.; Garg, V.K. Protein tyrosine phosphatase 1B as antidiabetic agents—A brief review. *Bioorg. Chem.* **2017**, *70*, 267–283. [[CrossRef](#)]
- Reddy, M.V.V.S.; Chakshusmathi, G.; Narasu, M.L. Small molecule inhibitors of PTP1B and TCPTP. *Int. J. Pharm. Phytopharmacol. Res.* **2012**, *1*, 287–291.

12. Rizvi, S.M.D.; Shakil, S.; Haneef, M. A simple click by click protocol to perform docking: Autodock 4.2 made easy for non-bioinformaticians. *EXCLI J.* **2013**, *12*, 831–857. [[PubMed](#)]
13. Wang, F.; Zhou, B. Toward the identification of a reliable 3D-QSAR model for the protein tyrosine phosphatase 1B inhibitors. *J. Mol. Struct.* **2018**, *1158*, 75–87. [[CrossRef](#)]
14. Ali, M.Y.; Kim, D.H.; Seong, S.H.; Kim, H.; Jung, H.A.; Choi, J.S.  $\alpha$ -Glucosidase and protein tyrosine phosphatase 1B inhibitory activity of plastoquinones from marine brown alga *Sargassum serratifolium*. *Mar. Drugs* **2017**, *15*, 368. [[CrossRef](#)] [[PubMed](#)]
15. Sotiriou, A. Novel Target for the Development of Drug for Type 2 Diabetes Mellitus. Ph.D. Thesis, Wageningen University, Wageningen, The Netherland, December 2016.
16. Na, B.; Nguyen, P.H.; Zhao, B.T.; Vo, Q.H.; Min, B.S.; Wo, M.H. Protein tyrosine phosphatase 1B (PTP1B) inhibitory activity and glucosidase inhibitory activity of compounds isolated from *Agrimonia pilosa*. *Pharm. Biol.* **2015**, *54*, 474–480. [[CrossRef](#)]
17. An, J.P.; Nguyen, P.H.; Ha, T.K.Q.; Kim, J.; Cho, T.O.; Oh, W.K. Protein tyrosine phosphatase 1B from the stem of *Akebia quinata*. *Molecules* **2016**, *21*, 1091. [[CrossRef](#)]
18. Wiese, J.; Aldemir, H.; Schmaljohann, R.; Gulde, T.A.M.; Imhoff, J.F. Asparentin B, a new inhibitor of Protein tyrosine phosphatase 1B. *Mar. Drugs* **2017**, *15*, 191. [[CrossRef](#)]
19. Mee, S.P.H.; Baldwin, J.E.; Cowley, A. Total synthesis of 5,5',6,6'-tetrahydroxy-3,3'-biindolyl, the proposed structure of a potent antioxidant found in Beetroot (*Beta vulgaris*). *Tetrahedron* **2004**, *60*, 3695–3712. [[CrossRef](#)]
20. Petterson, E.F.; Goddard, T.D.; Huang, C.C.; Couch, G.S.; Greenblatt, D.M.; Meng, E.C.; Ferrin, T.E. UCSF Chimera—A visualization system for exploratory research and analysis. *J. Comput. Chem.* **2004**, *25*, 1605–1612. [[CrossRef](#)] [[PubMed](#)]
21. Solomon, F.R.; Case, D.A.; Walker, R.C. An overview of the Amber biomolecular simulation package. *Wiley Interdiscip. Rev. Comput. Mol. Sci.* **2013**, *3*, 198–210. [[CrossRef](#)]
22. Miller, B.R.; McGee, T.D.; Swails, J.M.; Homeyer, N.; Gohlke, H.; Roitberg, A.E. MMPBSA.py: An efficient program for end-state free energy calculation. *J. Chem. Theory Comput.* **2012**, *8*, 3314–3321. [[CrossRef](#)]
23. Wang, J.; Wang, W.; Kollman, P.A.; Case, D.A. Automatic atom type and bond type perception in molecular mechanical calculations. *J. Mol. Graph. Model.* **2006**, *25*, 247–260. [[CrossRef](#)] [[PubMed](#)]
24. Mesquita, A.L.F.; Fernandes, J.R.M. Biochemical Properties and Possible Roles of Ectophosphatase Activities in Fungi. *Int. J. Mol. Sci.* **2014**, *15*, 2289–2304. [[CrossRef](#)] [[PubMed](#)]
25. Csank, C.; Makris, C.; Meloche, S.; Schröppel, K.; Rölinghoff, M.; Dignard, D.; Thomas, D.Y.; Whiteway, M. Derepressed hyphal growth and reduced virulence in a VH1 family-related protein phosphatase mutant of the human pathogen *Candida albicans*. *Mol. Biol. Cell* **1997**, *8*, 2539–2551. [[CrossRef](#)] [[PubMed](#)]
26. Downard, K.M.; Sheldon, J.C.; Bowie, J.H.; Lewis, D.E.; Hayes, R.N. Are the elusive ions mercaptomethyl (-CH<sub>2</sub>SH), hydroxymethyl (-CH<sub>2</sub>OH), and aminomethyl (-CH<sub>2</sub>NH<sub>2</sub>) detectable in the gas phase? A joint ab initio/experimental approach. *J. Am. Chem. Soc.* **1989**, *111*, 8112–8115. [[CrossRef](#)]
27. Trinajstić, N. Calculation of carbon-sulphur bond lengths. *Tetrahedron Lett.* **1968**, *9*, 1529–1532. [[CrossRef](#)]

